Fluoranthene-based triarylamines as hole-transporting and emitting materials for efficient electroluminescent devices†

Neha Kapoor and K. R. Justin Thomas*

Received (in Victoria, Australia) 1st June 2010, Accepted 5th July 2010
DOI: 10.1039/c0nj00415d

Electroluminescent materials based on the fluoranthene core and containing triarylamine segments were synthesized and characterized by IR, NMR, UV-Vis, and emission spectroscopic, electrochemical, and thermal studies. The electronic absorption and emission characteristics of the new functional materials were affected by the nature of the chromophore present on the fluoranthene nucleus. Incorporation of amine functionality red shifted the absorption and emission profiles significantly, while a marginal bathochromic shift was noticed for the cyano substituent. The redox propensity of the dyes was also altered by the nature of the substituents. The electron donating amino group imparted facile oxidation while the electron-withdrawing cyano unit rendered reduction capability. The decomposition temperatures (T_d) observed for the dyes are exceptionally high (406–527 °C). Electroluminescent devices incorporating two amines, *N*-(4-*tert*-butylphenyl)-*N*-(naphthalen-1-yl)-7,8,9,10-tetraphenylfluoranthen-3-amine (**7c**) and *N*-phenyl-*N*-(7,8,9,10-tetraphenylfluoranthen-3-yl)pyren-1-amine (**7d**) with the configurations ITO/**7c** or **7d** (40 nm)/TPBI or Alq_3 (40 nm)/LiF (1 nm)/Al (150 nm) were fabricated and displayed bright greenish yellow emission originating from the dyes.

Introduction

Molecular materials featuring multiple functional characteristics have been developed in recent years to use in electronic devices such as organic field effect transistors (OFETs), non-linear optics, solar cells and organic light emitting diodes (OLEDs).[1] OLEDs have gained significant interest due to their potential application in flat panel and full color range displays ever since the breakthrough demonstrations by Tang and Van Slyke[2] for vapor deposited multi-layered small molecule OLEDs (SMOLED) and Friend *et al.*[3] for spin coated polymer based OLEDs (PLED). Most of the electro-optical devices require materials featuring multiple functionalities. For instance, OLED requires organic materials possessing luminescent and charge transporting characteristics.[4,5] Embedding multiple functional entities in a single molecule is synthetically challenging and often leads to molecules dominating one function due to the imbalanced communication between them. In this direction dendrimers are being used as a suitable platform for rendering multiple functions at molecular level.[6] Multifunctional molecules are designed, synthesized and evaluated by many groups to diminish the steps in the cumbersome deposition of multi-layers of organic materials and reduce the production cost.[7] Evaluation of structure-property relationship in polyfunctional materials is also beneficial to improve the molecular design understanding for such applications.

Flat aromatic molecules and linear π-conjugated systems are highly fluorescent and exhibit potential applications in various electronic devices. However, an enfeebling and long standing problem with such systems is the molecular aggregation *via* π–π stacking which can suppress their emission in the solid state. Nonplanarity is the best solution to overcome the aggregation and nonplanar configuration can be easily achieved with the use of star shaped molecules or incorporation of bulky non-planar trigonal moieties in the molecules.[8] Shirota *et al.*[9–11] and Schmidt *et al.*[12,13] have reported several families of high T_g starburst aromatic amines which served as hole transporting materials for OLEDs. Inclusion of rigid polyaromatic segments has been additionally beneficial for increasing the thermal properties of the compounds.[14] Various molecules incorporated with polyphenyl-based dendrons (Müllen dendrons) have been demonstrated to be detrimental for the molecular aggregation or π–π stacking in the solid state.[15] Thus, conjugated dendrimers incorporating polyaromatics may be potential candidates for applications in electronic devices.

Fluoranthene segments have attracted a surge of interest recently as a promising scaffold for making high quality conducting polymers[16,17] and fluoranthene cored small molecules[18–21] were developed as effective materials for OLEDs, dye-sensitized solar cells and field effect transistors. In this paper, we report the synthesis of new fluoranthene derivatives containing multiple phenyl groups and an amine donor featuring an additional aromatic segment such as pyrene or naphthalene. As the newly developed materials contained amine functionality they were used as emitting hole transporters in OLEDs. This is in contrast to the earlier reports in which the fluoranthene derivatives were only applied as an emitting layer.[22] Also, the materials reported here show red-shifted emission in the greenish yellow region owing to the auxochromic effect of the amine unit. Additionally they exhibit very high thermal stability and display exceptionally high glass transition temperature owing to the presence of rigid structural units.

Department of Chemistry, Indian Institute of Technology Roorkee, Roorkee—247 667, India. E-mail: krjt8fcy@iitr.ernet.in; Fax: +91 1332 286202; Tel: +91 1332 285376

† Electronic supplementary information (ESI) available: Spectral data for the newly synthesized compounds. See DOI: 10.1039/c0nj00415d

Results and discussion

Synthesis and characterization

The fluoranthene containing bromo derivative, 3-bromo-7,8,9,10-tetraphenylfluoranthene required for the present study was made by an established route (Scheme 1).[23] In this method 1,3-diphenyl-2-propanone was condensed with the appropriate 5-bromoacenaphthylene-1,2-dione[24] to obtain the 3-bromo-7,9-diphenyl-8*H*-cyclopenta[*a*]acenaphthylene-8-one. This underwent Diels–Alder reaction with diphenyl acetylene in refluxing diphenyl ether to generate the desired precursor, 3-bromo-7,8,9,10-tetraphenylfluoranthene (**5b**). The syntheses of fluoranthene incorporated diarylamines (**7a–7d**) were accomplished by Pd-catalyzed C–N coupling strategy developed by Hartwig and co-workers.[25] To the best of our knowledge, animation reactions have not been demonstrated for the substrate which we used. For comparison, we have also synthesized 7,8,9,10-tetraphenylfluoranthene-3-carbonitrile(**6**) from 3-bromo-7,8,9,10-tetraphenylfluoranthene (**5b**) by means of a Rosenmund-Von Braun reaction[26] in which CuCN was used as reagent and DMF as solvent. This compound has been used in this work to evaluate the role of electron-withdrawing groups on the optical and electrochemical properties. The amine containing compounds are yellow in color and are soluble in common organic solvents and insoluble in methanol, hexane, and acetonitrile.

Optical properties

The absorption spectra of the compounds were recorded in dichloromethane and toluene. Representative absorption spectra recorded for the toluene solutions are presented in Fig. 1 along with the parent compounds for comparison. The data are listed in Table 1. The parent compound (**5a**) exhibited two absorption peaks centered at 295 and 373 nm, respectively originating from the π–π* transitions. It is interesting to note that the data is not significantly different from those observed for the basic unit fluoranthene (289 and 360 nm).[27] It suggests that outer phenyl rings do not extend the conjugation of the core dramatically. This is possibly due to the twisting of the phenyl groups out of the plane of the aromatic π-system which inhibits an effective π-conjugation with the fluoranthene core (see below for theoretical results). The absorption spectra were almost similar for **4**, **5a** and **5b**. Though the bromo substituent did not influence the absorption pattern in **5b**, the cyano

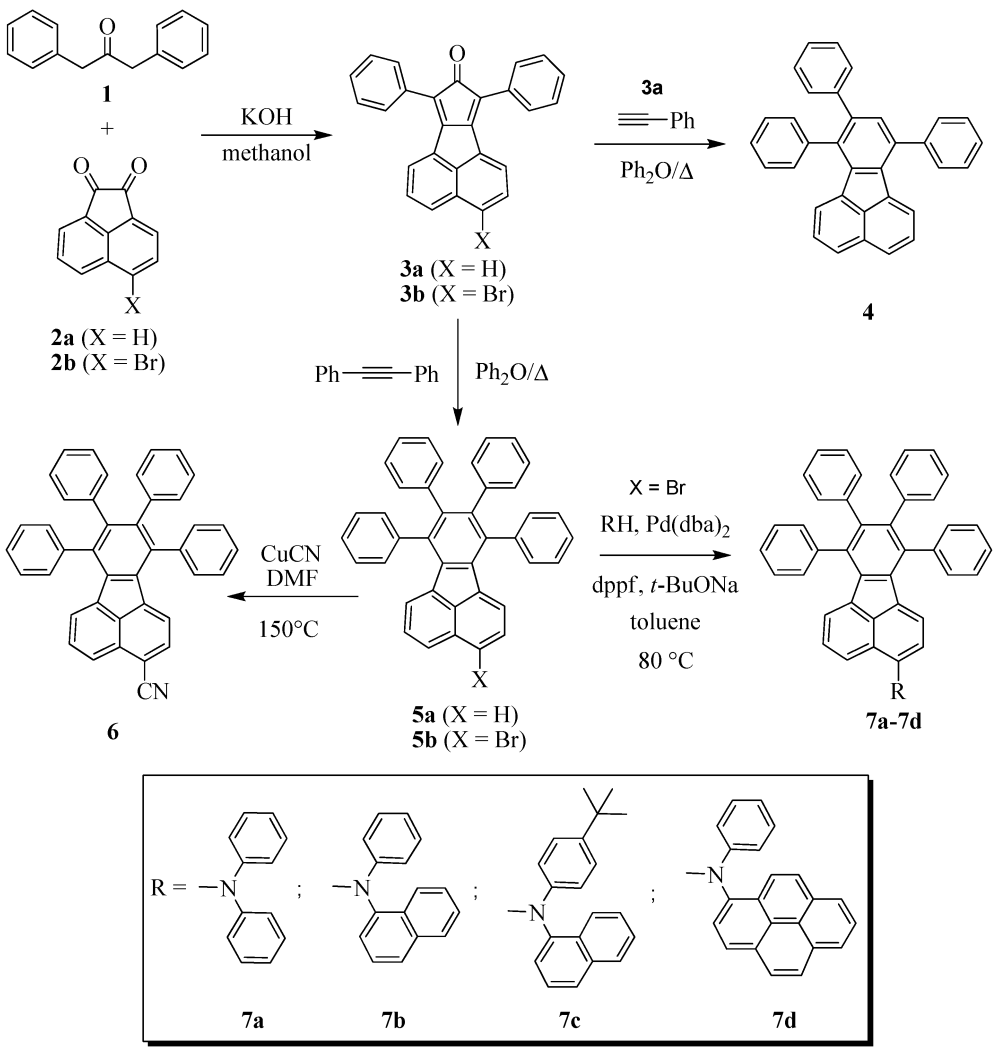

Scheme 1 Synthesis of the fluoranthene derivatives **4–7**.

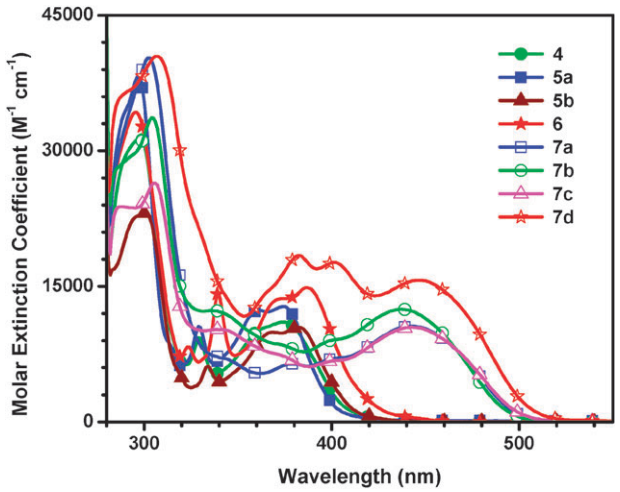

Fig. 1 Absorption spectra of the compounds (**4**, **5a**, **5b**, **6**, **7a–7d**) measured for toluene solutions.

bearing compound **6** showed bathochromic shift of 13 nm when compared to the parent compound (**5a**) which probably indicates a presence of charge transfer between the π-rich fluoranthene segment and the electron-withdrawing cyano unit. All the amine derivatives **7a–7d** showed a new prominent band located at 442–444 nm when compared to that of the parent compound (**5a**). The diarylamine could either act as a strong auxochrome or be involved in a facile charge transfer transition.[28,29] The appearance of absorption features in the higher wavelength has been noticed earlier for diarylamine substituted pyrene[28] or anthracene derivatives.[29] The triphenylamine, *N*,*N*-diphenylnaphthalen-1-amine and *N*,*N*-diphenylpyren-1-amine cores show absorption peaks at 303, 294 & 347 and 300 & 395 nm, respectively in dichloromethane solutions (see supporting information†).[30,31] The common peak at *ca.* 300 nm in these compounds seems to be originating from the diphenylamine chromophore. The absorptions in the higher wavelength region (347 and 395 nm) are attributed to the charge transfer transition from the amine donor to the aromatic acceptor segment. On a similar note the absorption peak appearing at the low energy side of the spectrum in the amine substituted compounds (**7a–7d**) is assigned to the charge transfer transition.

On comparing the absorption features of the amine derivatives few salient points emerge: (1) naphthyl phenyl amine derivative **7b** displays slighter hypsochromic shift (approx. 7 nm) than that of **7a**. This is because of the competitive delocalization of the lone pair of nitrogen by the naphthyl ring, (2) compound **7c** absorbs red-shifted (442 nm) when compared to that of **7b** and approximately the same as **7a** even though it contains a naphthyl unit. The reason for this might be the presence of a *t*-butyl group on the phenyl ring which probably alters the donor strength of the phenyl moiety, (3) absorption spectra of **7b** and **7c** show a hump at 335 nm which is due to the naphthalene unit and similarly two humps at 381 and 398 nm in the absorption spectrum of compound **7d** are probably arising due to the pyrene unit. The latter assignments are consistent with the fact that *N*,*N*-diphenylnaphthalen-1-amine and *N*,*N*-diphenylpyren-1-amine cores show absorption peaks at 347 and 395 nm, respectively.

It is evident from the data listed in Table 2, that the energy gap of these materials can be fine tuned by appropriate substitution in the 3rd position of the fluoranthene core. Substitution of an electron-withdrawing unit such as cyano widens the band gap while the electron-donating amine segment shrinks it. Among the amines the pyrene derivative **7d** displays the smaller band gap. All these points suggest that the fluoranthene core acts as a π–acceptor and the incorporation of amine functionality brings about dipolar character to the structure. Enhanced donor–acceptor interaction is expected to decrease the band gap.

Table 1 Photophysical properties of compounds

	Toluene			Dichloromethane		
Compound	λ_{max}/nm (ε_{max}/M^{-1} cm^{-1}) × 10^3)	λ_{em}/nm (Φ_F/%)	Stokes shift/cm^{-1}	λ_{max}/nm (ε_{max}/M^{-1} cm^{-1}) × 10^3)	λ_{em}/nm (Φ_F/%)	Stokes shift/cm^{-1}
4	298.0 (31.4), 329.0 (9.3), 374.0 (11.0)	460.5	4856	297.0 (28.6), 329.0 (7.9), 375.0 (9.9)	460.5 (36)	4880
5a	297.0 (38.3), 329.0 (10.6), 374.5 (12.8)	457 (37)	4987	295.0 (42.2), 328.0 (10.4), 373.0 (13.9)	459 (23)	5094
5b	300.5 (23.1), 334.0 (6.2), 382.5 (10.5)	469.5	4845	299.0 (28.4), 333.0, (5.9), 380.5 (12.3)	474 (12)	5184
6	295.5 (34.3), 323.5 (8.3), 339.0 (14.2), 387.5 (14.9)	494.5 (39)	5584	294.0 (36.5), 323.0 (8.7), 339.0 (14.6), 386.0 (16.2)	503 (7)	6026
7a	302.5 (40.3), 443.0 (10.6)	521.5 (41)	3398	300.0 (41.5) 442.0 (10.3)	544.5 (27)	4259
7b	304.0 (33.7), 335.5 (12.3), 437.0 (12.5)	518 (36)	3578	302.0 (35.3), 335.0 (12.5), 435.0 (13.0)	538.5 (26)	4418
7c	305.5 (26.4), 341.5 (10.2), 442.5 (10.5)	524 (37)	3515	303.0 (29.9), 339.5 (11.6), 443.0 (12.0)	549.5 (24)	4375
7d	306.5 (40.5), 382.5 (18.4), 401.0 (17.6), 446.5 (15.7)	530 (28)	3528	304.0 (37.8), 381.0 (17.2), 398.5 (16.2), 444.0 (14.9)	558 (11)	4601

Table 2 Electrochemical and thermal properties of the functional materials (**6**, **7a–7d**)

Compounds	E_{ox}, mV (ΔE_p, mV)	HOMO, eV	LUMO, eV	E_{0-0}/eV	T_m, °C	T_g, °C	T_d, °C
6	−1864.0	6.66	3.80	2.86	—	—	449
7a	492.0 (62)	5.29	2.84	2.45	345	198	469
7b	516.0 (67)	5.32	2.86	2.46	320	—	519
7c	460.0 (63)	5.26	2.82	2.44	—	192	502
7d	432.0 (67)	5.23	2.81	2.42	401	205	527

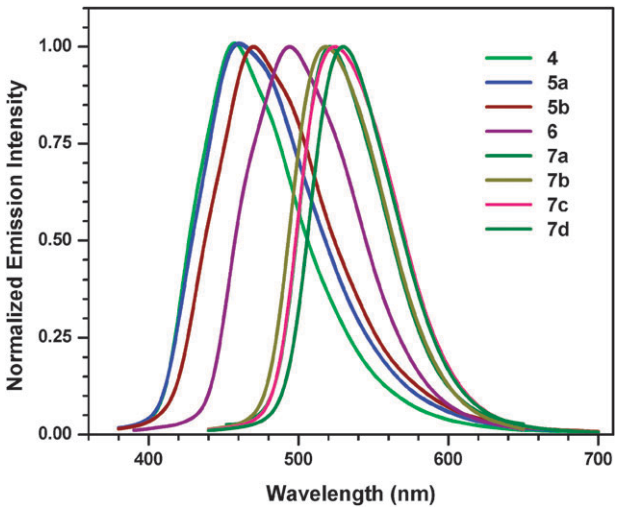

Fig. 2 Emission spectra of the compounds (**4**, **5a**, **5b**, **6**, **7a–7d**) measured in toluene.

The emission spectra recorded for the compounds in toluene are shown in Fig. 2. The emission peak appears in the range 460–558 nm. The emission characteristics were affected by the auxochromes. Incorporation of amine functionality red shifts the emission profiles. The emission colors of the amine derivatives are greenish yellow or yellow and are dependent on the nature of the diarylamine unit. The pyrene derivative displayed strong yellow emission. We have also recorded the emission of the vapor deposited films of **7c** and **7d** which showed emission peaks at 535 and 555 nm, respectively, and a more clear vibronic fine structure in the case of **7d** illustrating the rigidity and retention of the intermolecular segregation. The suppression of aggregation in the solid film is attributed to the presence of the polyphenylated chromophore which decrements tendency for molecular aggregation or π–π stacking.

No significant solvent dependent absorption behavior was observed for the compounds. However, the excited state solvatochromism observed for the compounds is noteworthy. The parent compound (**5a**) and **5b**, and **6** showed unaltered emission profiles on increasing the solvent polarity. On the contrary, the amine derivatives (**7a–7d**) displayed positive solvatochromism for the emission spectra. This indicates that the excited state of amine derivatives is more stable in polar solvent probably due to the separation of charges in the higher energy state.

Quantum yield was also measured for the compounds in toluene and dichloromethane (see Table 1). The fluorescence efficiency of the samples was high in non-polar solvents such as toluene and it decreased in dichloromethane. It has been noticed that the compounds that display comparatively lower oxidation potential exhibit less quantum yield when recorded in polar solvents. Thus, among amine derivatives (**7a–7d**), the pyrene derivative displays relatively lesser quantum efficiency in dichloromethane (Φ_F = 11%). This clearly indicates that the amino groups is effectively involved in an electron-transfer quenching of the excited states.

The Stokes shifts of the amine derivatives are small when compared to the parent compound **5a**, which probably indicates a more planar arrangement in the excited state than in the ground state. Similarly bromo derivative (**5b**) also displays a small Stokes shift when compared to the cyano derivative (**6**) because of the presence of a heavy bromine atom which makes the compound more rigid (Table 1). The Stokes shift is significantly larger in dichloromethane when compared to that in toluene indicating a possible role of dipole–dipole relaxation to the excited state.

Theoretical investigations

In order to understand the absorption characteristics of the dyes we have performed a theoretical calculation for the molecules **5a**, **6** and **7a** using density functional theory with the B3LYP functional and 6-31G(d,p) basis set. The prominent higher wavelength vertical transitions predicted by the theory are collected in Table 3 and the observed frontier molecular orbital diagrams are displayed in Fig. 3. The phenyl groups are significantly twisted from the fluoranthene core and display a lesser π-interaction. The higher wavelength absorption peaks observed for these compounds in toluene agree well with the theoretically forecast values except for a minor solvent role. For the parent compound **5a**, the intense band at 360 nm is thought to arise from the HOMO to LUMO electronic transition. The HOMO and LUMO orbitals of **5a** are π-type and mainly localized on the fluoranthene core. From this it can be safely concluded that the low energy transition observed for the parent compound **5a** originates from the fluoranthene based π–π* transition. For **6** a slight red-shift in absorption is proposed by theory which is faithfully observed in the experiment. The 380 nm vertical transition calculated for **6** shows approximately equal contributions from HOMO to LUMO and HOMO-1 to LUMO electronic transitions. The LUMO orbital in **6** is being contributed to from the cyano-fluoranthene segment and the HOMO and HOMO-1 orbitals are spread over the fluoranthene and phenyl segments. A red shift in the absorption is consequently attributed to the extension of conjugation in the molecule as there is a spread of orbitals over the larger section of the molecule. The diphenylamine containing derivative **7a** shows an intense vertical transition at 469 nm which is primarily composed of a HOMO to LUMO electron transfer. As the HOMO and LUMO for **7a** are contributed by the triarylamine and fluoranthene units, respectively, the transition at 469 nm is assigned to an amine to fluoranthene charge transfer.

Thermal properties

The thermal properties of the compounds were studied by both thermogravimetric analysis and differential scanning

Table 3 Predicted (TDDFT B3LYP/6-31G(d,p)) vertical transitions and their assignments

Compound	λ_{abs}, nm	f	Assignment
5a	375	0.02	HOMO-1 → LUMO (93%)
	360	0.25	HOMO → LUMO (92%)
6	411	0.02	HOMO → LUMO (53%)
			HOMO-1 → LUMO (40%)
	380	0.31	HOMO-1 → LUMO (54%)
			HOMO → LUMO (40%)
7	469	0.28	HOMO → LUMO (98%)
	376	0.09	HOMO-1 → LUMO (85%)

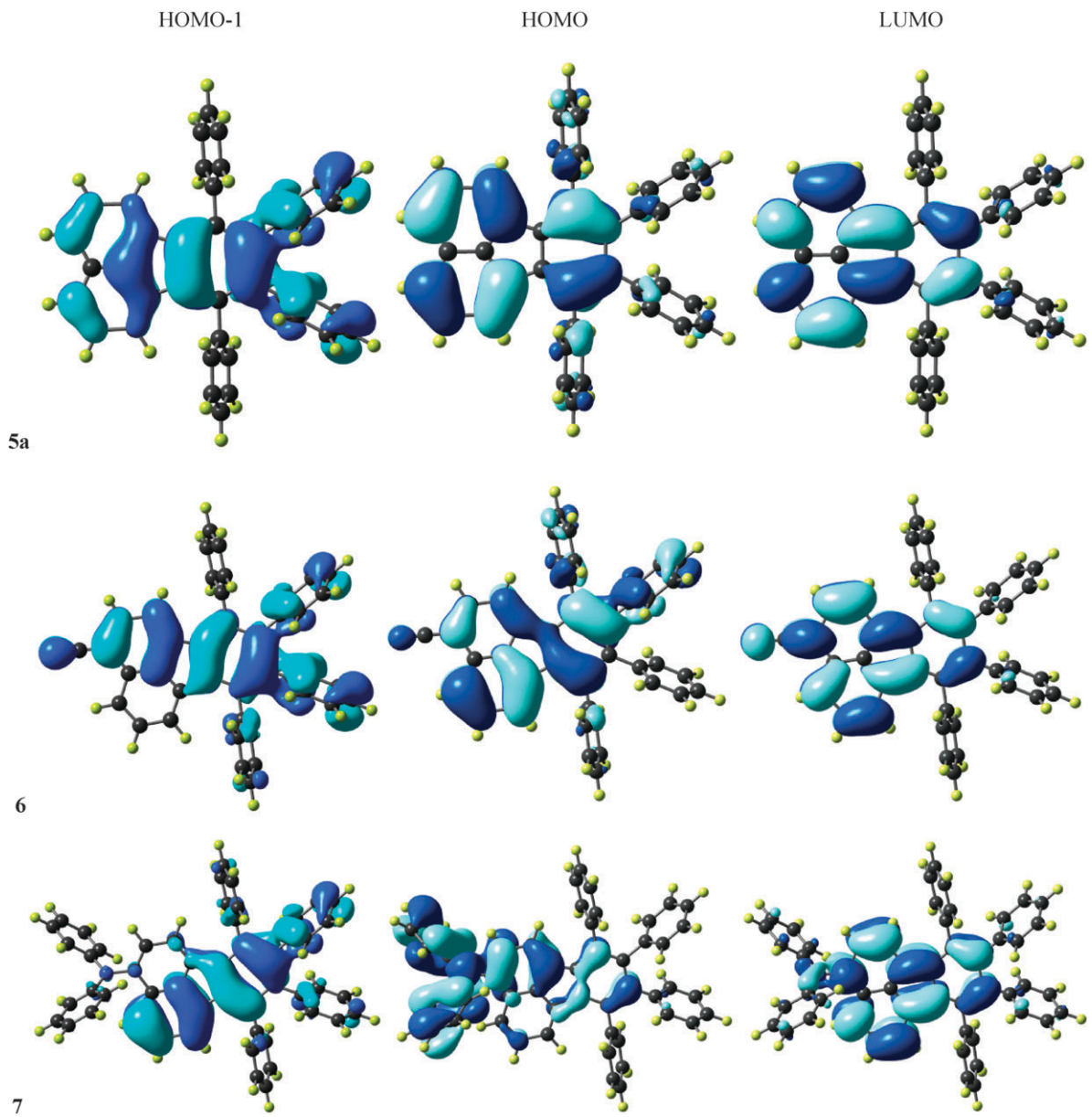

Fig. 3 Frontier molecular orbitals of the compounds **5a**, **6** and **7a**.

calorimetry measurements (see Table 2 for relevant parameters). All the compounds exhibited excellent thermal stability and the decomposition temperatures are in the range of 406–527 °C. The marked thermal robustness of the compounds is attributed to the fused polyaromatic architecture. The thermal stability trend observed for compounds **4**, **5a**, **5b** and **6** may be assigned to the differences in the number of non-hydrogen atoms and molecular heaviness. Diarylamine derivatives (**7a–7d**) display thermal decomposition temperatures above 450 °C and the order of stability is **7a** < **7c** < **7b** < **7d**. Among the naphthylamine derivatives (**7b** and **7c**) improved thermal stability is observed for **7b**. This difference probably arises due to the presence of the *tert*-butyl group in **7c** which makes the molecule floppy. The stability order realized based on the diarylamine units, diphenylamine (**7a**) < 1-naphthylphenylamine (**7b** & **7c**) < 1-pyrenylphenylamine (**7d**), is in accordance with the earlier observations which revealed that molecular materials containing flat polyaromatic extended skeletons were prone to resisting thermal degradation. Glass transition temperatures of **7c** and **7d** were recorded as 192 °C and 205 °C, respectively. The present amine derivatives (**7a–7d**) were found to show exceptionally higher thermal stability and a prolonged glassy state than the reported blue emitting fluoranthene derivatives, 7,10-diphenyl-8-(1-naphthyl) fluoranthene [DPNF] and 7,10-diphenyl-8-(9-phenanthrenyl)fluoranthene[DPPF].[22] This clearly highlights the importance of amine functionality in improving the emission and thermal properties.

Electrochemical properties

The redox propensity of the compounds was examined in 2×10^{-4} M dichloromethane solutions by cyclic and

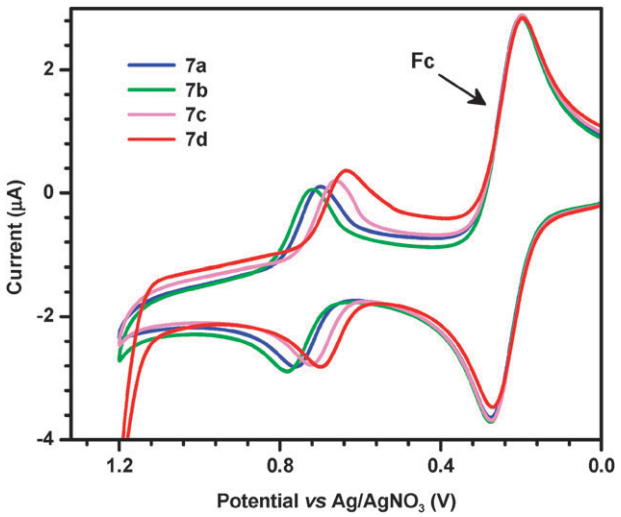

Fig. 4 Cyclic voltammograms recorded for the amine functionalized derivatives (**7a–7d**) in dichloromethane solutions (concentration: 2.0×10^{-4} M; scan rate: 100 mV s^{-1}; supporting electrolyte: TBAHP).

differential pulse voltammetric methods. The cyclic voltammograms recorded for the amine derivatives (**7a–7d**) with the internal standard ferrocene are displayed in the Fig. 4. The pertinent parameters are collected in Table 2. All the amines exhibited one quasi-reversible oxidation couple followed by one irreversible oxidation peak. It is reasonable to assume that the quasi-reversible oxidation wave arises from the amine functionality while the irreversible oxidation may originate from the fluoranthene core. It is interesting to note that this irreversible wave attributable to the fluoranthene core is not observed for the bromo (**5b**) and cyano derivatives (**6**). Probably, the electron attracting nature of these groups either positively shifts this potential and the wave probably appears outside the electrochemical window or the core less prone to oxidation. This argument is further supported by the fact that the cyano derivative (**6**) shows a quasi-reversible reduction couple.

The orbital energies, deduced from the oxidation potentials and absorption edge, are also listed in Table 2. The HOMO energy levels were observed to be 6.66, 5.29, 5.32, 5.26 and 5.23 eV for **6**, **7a**, **7b**, **7c**, and **7d**, respectively. It was revealed that the electron withdrawing substituent lowers the HOMO energy level whereas the electron donating group increases the HOMO energy level and decreases the LUMO energy resulting in a smaller band gap. The conclusions about the band gap derived from the optical spectra can be corroborated with these findings (*vide supra*). All the amine derivatives show comparable band gaps, out of which the pyrene derivative (**7d**) shows a comparatively low band gap, which is evident from the red-shifted absorption profile and cathodically shifted oxidation potential.

Electroluminescence and OLED performance

As the amine derivatives have displayed favorable electrochemical, thermal and emission properties, we further examined two selected derivatives (**7c** and **7d**) as hole transporting emitting materials in double layer OLEDs. We have used both

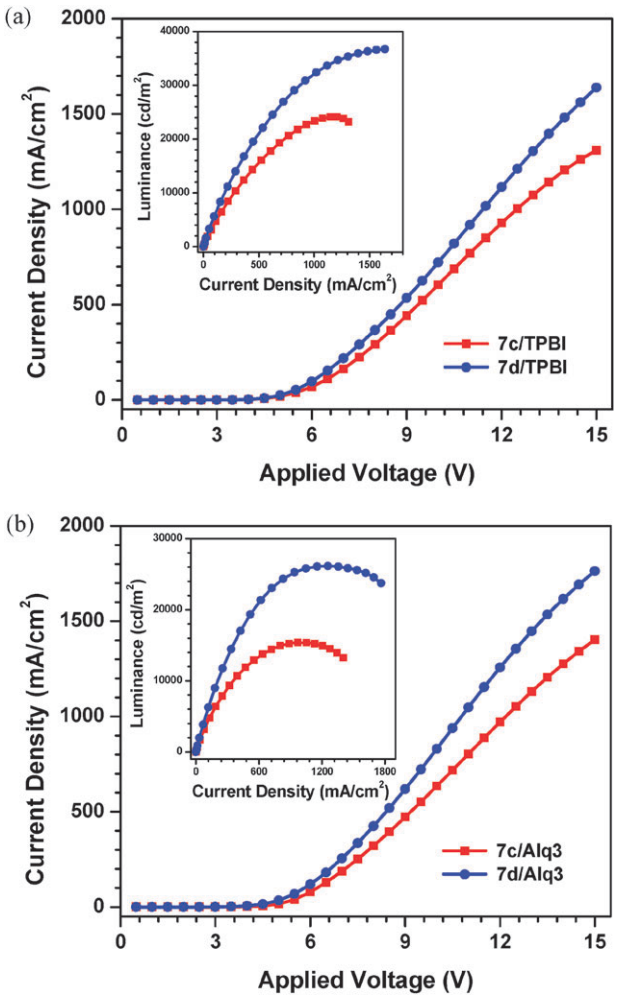

Fig. 5 *I–V–L* characteristics of the devices fabricated using (a) TPBI or (b) Alq_3 as electron transporting layer.

1,3,5-tris(*N*-phenylbenzimidazol-2-yl)benzene (TPBI) and aluminium tris-8-hydroxyquinoline (Alq_3) as electron transporting materials to effect the optimization of charge balance in the devices. The devices had the configuration as ITO/**7c** (40 nm)/TPBI or Alq_3 (40 nm)/LiF (1 nm)/Al (150 nm) [Device I] and ITO/**7d** (40 nm)/TPBI or Alq_3 (40 nm)/LiF (1 nm)/Al (150 nm) [Device II]. Fig. 5 shows the current–voltage–luminance (*I–V–L*) characteristics of the fabricated devices, and their device characteristics at 100 and 20 mA cm^{-2} are listed in Table 4. In general, the TPBI serves as a better electron transporting material for these devices than Alq_3, which is clearly evident from the better efficiency and brightness observed for the TPBI based devices. Particularly, device II with TPBI as an electron transporting layer showed the highest external quantum efficiency 1.86%, current efficiency 6.73 cd A^{-1} and power efficiency 4.37 lm/W at a voltage of 4.85 V and a current density of 20 mA cm^{-2}. The improved performance for pyrene containing the dye-TPBI device is attributed to the larger barrier for the injection of holes from the dyes (**7d**) to TPBI (0.97 eV) when compared to the corresponding barrier (0.86 eV) at the interface of **7d**-Alq_3 (Fig. 6). This probably enhances the possibility of recombination and confinement of the exciton in the emitting layer.

Table 4 Electroluminescence characteristics of the devices constructed from **7c** and **7d**

	7c/TPBI	**7c**/Alq_3	**7d**/TPBI	**7d**/Alq_3
λ_{em} (fwhm), nm	534 (70)	534 (74)	558 (56)	558 (62)
Max. brightness (Cd/m^2)	24120	15390	36750	26140
CIE (x, y)	0.34, 0.60	0.34, 0.59	0.42, 0.55	0.41, 0.55
External quantum efficiency (%) at (100/20 mA cm^{-2})	1.21/1.48	1.09/1.23	1.60/1.86	1.53/1.66
Power efficiency (lm/W) at (100/20 mA cm^{-2})	2.132/3.300	1.981/2.718	3.026/4.373	2.933/4.010
Current efficiency (Cd/A) at (100/20 mA cm^{-2})	4.315/5.287	3.904/4.397	5.801/6.733	5.413/5.889
Voltage/V at (100/20 mA cm^{-2})	6.37/5.04	6.21/5.09	6.03/4.85	5.81/4.62
Brightness (Cd/m^2) at (100/20 mA cm^{-2})	4290/1050	3860/870	5790/1330	5380/1170

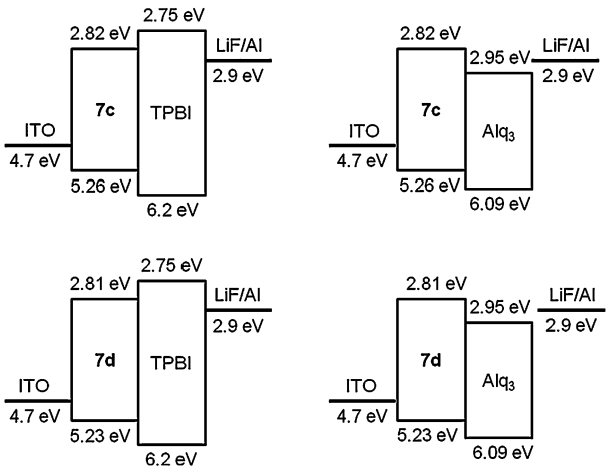

Fig. 6 Energy level diagram of the four devices fabricated using the dyes **7c** and **7d** with TPBI and Alq_3.

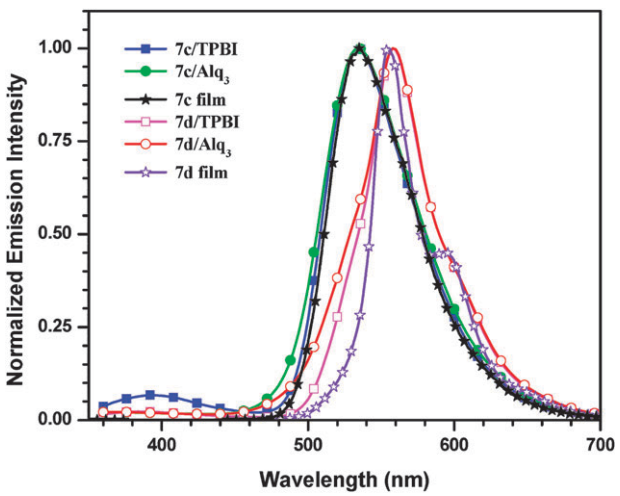

Fig. 7 Comparison of EL spectra observed for the devices with the PL spectra recorded for the thin films.

The leaking of holes into the TPBI layer is also confirmed by the residual TPBI based emission observed in the EL (Fig. 7).

EL spectra show peaks at 534 and 558 nm for **7c** and **7d** based devices, respectively. CIE coordinates for **7c** and **7d** based devices indicated green and yellow emissions, respectively. This suggests that the emission is originating from the dye. Although fluorene bridged fluoranthene derivatives have been applied in electroluminescent devices, they were found to be blue emitting in the electroluminescent devices.[32] In this work, by using amine functionality, we have shown that the emission color can be tuned to green and yellow depending on the nature of the diarylamine tethered with the fluoranthene core.

Conclusions

In summary, we have synthesized electroluminescent materials based on a fluoranthene core integrated with a polyphenylated dendron-like structure. Incorporation of diarylamine red shifts the absorption as well as the emission profiles. All four amine derivatives are potential molecular materials displaying unique absorption, emission, thermal and electrochemical properties. Further, we have also demonstrated that these derivatives can function as efficient hole transporting and emitting material in OLEDs. Particularly, the device fabricated using the pyrene containing derivative, **7d**, displayed promising external quantum efficiency 1.86% and maximum brightness 36750 cd m^{-2} with TPBI as an electron transporting layer, which appear to be rather high among the previously reported carbazole based derivatives capable of green or yellow emission and hole transporting.[33]

Experimental

General methods

All commercially available materials were used as obtained from their sources. Dichloromethane (DCM) and toluene were distilled from phosphorus pentoxide. All chromatographic separations were carried out with hexane : DCM on silica gel (60–120 mesh, Rankem).

^1H and ^{13}C NMR spectra were recorded on a Bruker AV500 O FT-NMR spectrometer operating at 500 and 125 MHz, respectively in $CDCl_3$ and $(CD_3)_2SO$ (chemical shifts (δ) in ppm and coupling constants (J) in Hz). Me_4Si (0.00 ppm) served as internal standard, or residual signals for $CHCl_3$ (^{1}HNMR, δ = 7.26; ^{13}CNMR, δ = 77.36 ppm) or DMSO (^{1}HNMR, δ = 2.5 ppm; ^{13}CNMR δ = 40.45 ppm). Mass spectra were recorded on a JMS-700 double focusing mass spectrometer (JEOL, Tokyo, Japan) or a Bruker ESI TOF mass spectrometer. IR spectra were measured on NEXUS FT-IR (THERMONICOLET). The electronic absorption spectra were obtained with an Evolution 600, Thermo Scientific UV-Vis spectrophotometer in dichloromethane and toluene solutions. Emission spectra were recorded in dichloromethane and toluene with a Fluorolog®3 spectrofluorimeter. The fluorescence quantum yields (Φ_F) were determined using the classical formula: $\Phi_s = (\Phi_r \times A_r \times I_s \times \eta_s^2)/(A_s \times I_r \times \eta_r^2)$

where A is the absorbance at the excitation wavelength, I is the integrated area under the fluorescence curve and η is the refraction index. Subscripts r and s refer to the reference and to the sample of unknown quantum yield, respectively. Coumarin 6 in ethanol ($\Phi_F = 0.78$) or coumarin 1 (($\Phi_F = 0.99$) in ethyl acetate was used as the reference. The samples were excited either at 340 nm (for coumarin 1 reference) or 420 nm (for coumarin 6 reference) during the quantum yield measurements. Qualitative emission spectra of the samples were obtained by exciting at the absorption maximum. Cyclic voltammetry experiments were performed with a CH Instruments electrochemical analyzer. All measurements were carried out at room temperature with a conventional three-electrode configuration consisting of a glassy carbon working electrode, a platinum wire auxiliary, and a nonaqueous acetonitrile $Ag/AgNO_3$ reference electrode. The $E_{1/2}$ values were determined as $(E_p^a + E_p^c)/2$, where E_p^a and E_p^c are the anodic and cathodic peak potentials, respectively. The potentials are quoted against ferrocene internal standard. The solvent in all experiments was dichloromethane and the supporting electrolyte was 0.1 M tetrabutylammonium hexafluorophosphate. Thermal studies such as TGA-DTA-DTG measurements were performed on a Perkin-Elmer (Pyris Diamond) at a heating rate of 10 °C min^{-1} under a nitrogen atmosphere.

OLED fabrication and performance evaluation

Prepatterned ITO substrates with an effective individual device area of 3.14 mm^2 were cleaned as described in a previous report.[34] The amine derivatives (**7c** or **7d**) acting as hole transporting emitting layers were first deposited (40 nm) on the ITO substrate by vapor deposition. Then 40-nm-thick Alq_3 or a TPBI layer as an electron transport layer was deposited. Finally, a thin layer of LiF (10 Å) followed by aluminium (1500 Å) was deposited as the cathode. The I–V curve was measured on a Keithley 2400 Source meter in an ambient environment. Light intensity was measured with a Newport 1835 optical meter.

Computational details

The ground state geometry of the compounds at the gas phase were optimized using the density functional theory method with the B3LYP functional in conjugation with the basis set 6-31G(d,p) as implemented in the Gaussian 09 package.[35] The default options for the self-consistent field (SCF) convergence and threshold limits in the optimization were used. The electronic transitions were calculated using the time-dependent DFT (B3LYP) theory and the 6-31G(d,p) basis set. Even though the time-dependent DFT method less accurately describes the states with charge-transfer nature, the qualitative trends in the TDDFT results can still offer correct physical insights. At least 10 excited states were calculated for each molecule.

Synthesis

The parent compounds 7,8,10-triphenylfluoranthene[36] (**4**) and 7,8,9,10-tetraphenylfluoranthene[23] (**5a**) were synthesized by the method reported in the literature.

Synthesis of 3-bromo-7,8,9,10-tetraphenylfluoranthene (5b)

A mixture of 3-bromo-7,9-diphenyl-8*H*-cyclopenta[*a*]-acenaphthylen-8-one (**3b**) (1 g, 2.3 mmol) and diphenylacetylene (0.45 g, 2.53 mmol) in diphenylether (5 ml) were heated to 220 °C and stirred for 7 h. After completion of the reaction, it was quenched by adding hexane. A gray precipitate was formed. It was filtered and adsorbed on silica gel for subsequent purification by column chromatography. The desired product was separated by eluting with a 5 : 1 hexane–dichloromethane mixture as a pale yellow color solid. Yield: 0.96 g (71%). ^{1}H NMR (DMSO, 500 MHz, ppm): δ 7.85 (d, J = 8.5 Hz, 1 H)), 7.69 (d, J = 7.5 Hz, 1 H), 7.49 (t, J = 7.8 Hz, 1 H), 7.30–7.38 (m, 10 H), 6.96–6.98 (m, 4 H), 6.90 (t, J = 7.8 Hz, 4 H), 6.82–6.85 (m, 2 H), 6.42 (d, J = 7.5 Hz, 1 H), 6.25 (d, J = 7.5 Hz, 1 H). ^{13}C ($CDCl_3$, 125 MHz, ppm): δ 141.11, 141.04, 139.68, 139.64, 139.52, 137.38, 137.29, 136.85, 136.37, 136.18, 135.90, 134.48, 131.21, 131.00, 129.98, 129.93, 129.43, 128.85, 128.27, 127.07, 127.05, 126.69, 125.76, 125.54, 123.89, 123.72, 121.88. IR (KBr, cm^{-1}): 3056, 1601, 1495, 1442, 1421, 837, 818, 769, 699.

Synthesis of 7,8,9,10-tetraphenylfluoranthene-3-carbonitrile (6)

A mixture of 3-bromo-7,8,9,10-tetraphenylfluoranthene (**5b**) (0.73 g, 1.25 mmol) and cuprous cyanide (0.16 g, 1.87 mmol) and dimethylformamide (10 mL) were placed in a round bottom flask and heated at 150 °C with efficient stirring for 48 h. The mixture was poured into 10 ml of ammonia solution to yield a dark yellow precipitate. It was filtered and washed thoroughly with water. This crude product was further purified by column chromatography using a 2 : 3 mixture of dichloromethane and hexane to yield a pale yellow solid. Yield: 0.24 g (36%). ^{1}H NMR ($CDCl_3$, 500 MHz, ppm): δ 7.93 (d, J = 8.5 Hz, 1 H), 7.67 (d, J = 7.5 Hz, 1 H), 7.41 (t, J = 7.8 Hz, 1 H), 7.28–7.35 (m, 10 H), 6.85–6.91 (m, 10 H), 6.61 (d, J = 7 Hz, 1H), 6.55 (d, J = 7.0 Hz, 1 H); ^{13}C NMR ($CDCl_3$, 125 MHz, ppm): δ 141.63, 140.66, 138.44, 138.37, 138.23, 138.16, 137.58, 136.86, 136.36, 136.18, 134.40, 133.44, 131.92, 130.21, 130.14, 129.29, 128.93, 128.86, 128.11, 127.55, 127.51, 126.48, 126.38, 125.90, 124.85, 123.68, 123.12, 120.95, 116.90, 107.22. IR (KBr, cm^{-1}): 3056, 2215, 1603, 1496, 1438, 1418, 765, 698.

General synthesis of the amine derivatives

The amine substituted fluoranthene derivatives (**7a–7d**) were obtained by essentially following a similar procedure utilizing the C–N coupling reaction involving the palladium catalyst. An illustrative description is given below for the synthesis of compound **7a**.

Synthesis of *N*,*N*,7,8,9,10-hexaphenylfluoranthen-3-amine (**7a**). A mixture of 3-bromo-7,8,9,10-tetraphenylfluoranthene (1.17 g, 2 mmol), diphenylamine (0.41 g, 2.4 mmol), $Pd(dba)_2$ (0.023 g, 0.04 mmol), dppf (0.022 g, 0.04 mmol), sodium *tert*-butoxide (0.29 g, 3 mmol), and toluene (15 ml) was placed in a pressure tube. It was heated at 80 °C and stirred for 48 h. After completion of the reaction, as evidenced by the disappearance of 3-bromo-7,8,9,10-tetraphenylfluoranthene, it was quenched by the addition of water and extracted with dichloromethane. The combined extracts were washed with

brine solution and dried over anhydrous Na_2SO_4. Rotary evaporation of the extracts gave the crude product which on column chromatography purification using 1 : 4 hexane–dichloromethane mixtures produced a yellow solid. Yield: 1.2 g (89%). ^{1}H NMR ($CDCl_3$, 500 MHz, ppm): δ 7.53 (d, J = 8.5 Hz, 1 H), 7.27–7.32 (m, 8 H), 7.21–7.23 (m, 1 H), 7.16 (t, J = 8.0 Hz, 4 H), 7.04–7.07 (m, 1 H), 7.01 (d, J = 7.5 Hz, 4 H), 6.84–6.96 (m, 14 H), 6.49 (d, J = 7.0 Hz, 1 H), 6.46 (d, 7.5 Hz, 1 H). ^{13}C ($CDCl_3$, 125 MHz, ppm): δ = 148.97, 144.46, 140.67, 140.25, 139.88, 139.81, 137.20, 136.86, 136.77, 136.55, 136.15, 133.74, 131.33, 131.28, 130.06, 130.04, 129.11, 128.16, 127.35, 127.29, 126.96, 126.90, 126.87, 126.62, 125.43, 124.17, 124.12, 123.24, 122.99, 122.16. ESI-TOF MS: Calcd for $C_{52}H_{35}N$: 673.2770. Found: 674.2832 $(M+H)^+$.

N-(Naphthalen-1-yl)-*N*,7,8,9,10-pentaphenylfluoranthen-3-amine (**7b**) Yellow solid. Yield: 75%. ^{1}H NMR ($CDCl_3$, 500 MHz, ppm): δ 7.98 (d, J = 9.0 Hz, 1 H), 7.84 (d, J = 8.0 Hz, 1 H), 7.67 (d, J = 8.5 Hz, 1 H), 7.61 (d, J = 8.0 Hz, 1 H), 7.42 (t, J = 7.3 Hz, 1 H), 7.27–7.36 (m, 7 H), 7.17–7.25 (m, 6 H), 7.09–7.12 (m, 2 H), 7.03–7.06 (m, 1 H), 6.79–6.92 (m, 14 H), 6.51 (d, J = 7.0 Hz, 1 H), 6.35 (d, J = 7.5 Hz, 1 H). ^{13}C ($CDCl_3$, 125 MHz, ppm): δ = 150.73, 145.55, 145.09, 140.67, 140.12, 139.92, 139.86, 139.82, 137.18, 136.91, 136.65, 136.48, 136.21, 135.22, 135.12, 133.01, 131.35, 131.29, 130.30, 130.06, 129.22, 128.98, 128.39, 128.17, 128.12, 127.26, 126.91, 126.81, 126.61, 126.37, 126.33, 126.09, 126.06, 125.91, 125.82, 125.41, 124.67, 124.28, 124.20, 124.06, 123.34, 123.18, 121.52, 121.34. ESI-TOF MS: Calcd for $C_{56}H_{37}N$: 723.2926. Found: 724.2981 $(M+H)^+$.

N-(4-*tert*-Butylphenyl)-*N*-(naphthalen-1-yl)-7,8,9,10-tetraphenylfluoranthen-3-amine (**7c**) Yellow solid. Yield: 84%. ^{1}H NMR ($CDCl_3$, 500 MHz, ppm): δ 7.99 (d, J = 8.0 Hz, 1 H), 7.83 (d, J = 8.5 Hz, 1 H), 7.65 (d, J = 8.0 Hz, 1 H), 7.59 (d, J = 8.0 Hz, 1 H), 7.39–7.42 (m, 1 H), 7.27–7.33 (m, 6 H), 7.21–7.25 (m, 4 H), 7.16–7.17 (m, 2 H), 7.10 (d, J = 9.0 Hz, 2 H), 7.02–7.03 (m, 1 H), 6.82–6.91 (m, 11 H), 6.76 (d, J = 8.0 Hz, 3 H), 6.49 (d, J = 7.5 Hz, 1 H), 6.36 (d, J = 8.0 Hz, 1 H), 1.25 ppm (s, 9 H); ^{13}C ($CDCl_3$, 125 MHz, ppm): δ 148.10, 146.06, 145.47, 144.36, 140.60, 139.94, 139.85, 137.11, 136.78, 136.53, 136.43, 136.22, 135.17, 132.55, 131.34, 131.29, 130.27, 130.07, 128.31, 128.13, 128.09, 127.04, 126.86, 126.76, 126.58, 126.33, 126.19, 126.04, 125.97, 125.77, 125.65, 125.52, 125.36, 124.37, 124.31, 124.17, 124.06, 123.09, 121.48, 34.14, 31.42. FAB MS: Calcd for $C_{60}H_{45}N$: 779.3552. Found: 780.3 $[M+H]^+$.

N-Phenyl-*N*-(7,8,9,10-tetraphenylfluoranthen-3-yl)pyren-1-amine (**7d**) Orange solid. Yield: 75%. ^{1}H NMR ($CDCl_3$, 500 MHz, ppm): δ 8.18 (d, J = 9.0 Hz, 1 H), 8.15 (d, J = 7.5 Hz, 1 H), 8.03–8.08 (m, 2 H), 8.01 (d, J = 4.5 Hz, 2 H). 7.96 (t, J = 8.0 Hz, 1 H), 7.85 (d, J = 9.5 Hz, 1 H), 7.73 (d, J = 8.0 Hz, 1 H), 7.66 (d, J = 8.0 Hz, 1 H), 7.28–7.31 (m, 5 H), 7.19 (t, J = 7.5 Hz, 2 H), 7.11–7.14 (m, 3 H), 7.02–7.05 (m, 1 H), 6.81–6.92 (m, 16 H), 6.52 (d, J = 7.0 Hz, 1 H), 6.34 (d, J = 7.5 Hz, 1 H); ^{13}C ($CDCl_3$, 125 MHz, ppm): δ 150.89, 145.75, 142.56, 140.68, 140.13, 139.90, 139.84, 139.77, 137.19, 136.97, 136.67, 136.47, 136.21, 135.16, 133.03, 131.34, 131.27, 131.06, 130.05, 130.01, 129.12, 129.09, 128.16, 128.10, 127.85, 127.30, 127.24, 126.90, 126.86, 126.78, 126.60, 126.52, 126.41, 126.33, 126.20, 125.72, 125.40, 125.19, 125.16, 125.01, 124.86, 124.26, 124.11, 123.29, 123.23, 121.58, 121.48. FAB MS: Calcd for $C_{62}H_{39}N$: 797.3083. Found: 797.2 $[M]^+$.

Acknowledgements

We thank the Council of Scientific and Industrial Research (CSIR), New Delhi for financial support (grant no. 01(2111)/07/EMR-II). NK acknowledges UGC for a research fellowship. We are also thankful to Prof. J. T. Lin, Academia Sinica, Taipei for the OLED characterization facility.

References

1 D. Braga and G. Horowitz, *Adv. Mater.*, 2009, **21**, 1473; W. H. Howie, F. Claeyssens, H. Miura and L. M. Peter, *J. Am. Chem. Soc.*, 2008, **130**, 1367; Z. Zhao, X. Xu, H. Wang, P. Lu, G. Yu and Y. Liu, *J. Org. Chem.*, 2008, **73**, 594; K. Kreger, M. Bäte, C. Neuber, H.-W. Schmidt and P. Strohriegl, *Adv. Funct. Mater.*, 2007, **17**, 3456; P. A. Sullivan, A. J. P. Akelaitis, S. K. Lee, G. McGrew, S. K. Lee, D. H. Choi and L. R. Dalton, *Chem. Mater.*, 2006, **18**, 344.
2 C. W. Tang and S. A. Van Slyke, *Appl. Phys. Lett.*, 1987, **51**, 913.
3 J. H. Burroughes, D. D. C. Bradley, A. R. Brown, R. N. Marks, K. Mackay, R. H. Friend, P. L. Burn and A. B. Holmes, *Nature*, 1990, **347**, 539.
4 S. Jiao, Y. Liao, X. Xu, L. Wang, G. Yu, L. Wang, Z. Su, S. Ye and Y. Liu, *Adv. Funct. Mater.*, 2008, **18**, 2335.
5 Y.-L. Liao, W.-Y. Hung, T.-H. Hou, C.-Y. Lin and K.-T. Wong, *Chem. Mater.*, 2007, **19**, 6350.
6 W. W. H. Wong, D. J. Jones, C. Yan, S. E. Watkins, S. King, S. A. Haque, X. Wen, K. P. Ghiggino and A. B. Holmes, *Org. Lett.*, 2009, **11**, 975; M. Saleh, M. Baumgarten, A. Mavrinskiy, T. Schäfer and K. Müllen, *Macromolecules*, 2010, **43**, 137.
7 C.-H. Chen, W.-S. Huang, M.-Y. Lai, W.-C. Tsao, J. T. Lin, Y.-H. Wu, T.-H. Ke, L.-Y. Chen and C.-C. Wu, *Adv. Funct. Mater.*, 2009, **19**, 2661.
8 Q.-X. Tong, S.-L. Lai, M.-Y. Chan, K.-H. Lai, J.-X. Tang, H.-L. Kwong, C.-S. Lee and S.-T. Lee, *Chem. Mater.*, 2007, **19**, 5851.
9 Y. Shirota, T. Kobata and N. Noma, *Chem. Lett.*, 1989, 1145; A. Higuchi, H. Inada, T. Kobata and Y. Shirota, *Adv. Mater.*, 1991, **3**, 549.
10 H. Inada and Y. Shirota, *J. Mater. Chem.*, 1993, **3**, 319.
11 K. Katsuma and Y. Shirota, *Adv. Mater.*, 1998, **10**, 223.
12 M. Thelakkat and H.-W. Schmidt, *Adv. Mater.*, 1998, **10**, 219.
13 M. Thelakkat, C. Schmitz, C. Hohle, P. Strohriegl, H.-W. Schmidt, U. Hofmann, S. Schloter and D. Haarer, *Phys. Chem. Chem. Phys.*, 1999, **1**, 1693.
14 J. Li, D. Liu, Y. Li, C.-S. Lee, H.-L. Kwong and S. Lee, *Chem. Mater.*, 2005, **17**, 1208.
15 K. R. J. Thomas, M. Velusamy, J. T. Lin, C. H. Chuen and Y. T. Tao, *J. Mater. Chem.*, 2005, **15**, 4453; C. Huang, C.-G. Zhen, S. P. Su, K. P. Loh and Z.-K. Chen, *Org. Lett.*, 2005, **7**, 391.
16 J. D. Debad and A. J. Bard, *J. Am. Chem. Soc.*, 1998, **120**, 2476.
17 J. Xu, J. Hou, S. Zhang, Q. Xiao, R. Zhang, S. Pu and Q. Wei, *J. Phys. Chem. B.*, 2006, **110**, 2643.
18 S. Kawano, C. Yang, M. Ribas, S. Baluschev, M. Baumgarten and K. Müllen, *Macromolecules*, 2008, **41**, 7933.
19 E. F. Fabrizio, A. Payne, N. E. Westlund, A. J. Bard and P. P. Magnus, *J. Phys. Chem. A*, 2002, **106**, 1961.
20 X. Ma, W. Wu, Q. Zhang, F. Guo, F. Meng and J. Hua, *Dyes and Pigments*, 2009, **82**, 353.
21 Q. Yan, Y. Zhou, B.-B. Ni, Y. Ma, J. Wang, J. Pei and Y. Cao, *J. Org. Chem.*, 2008, **73**, 5328.
22 S.-K. Kim, J.-Y. Jaung and J.-W. Park, *Mol. Cryst. Liq. Cryst.*, 2008, **491**, 122.
23 Y.-T. Wu, T. Hayama, K. K. Baldridge, A. Linden and J. S. Siegel, *J. Am. Chem. Soc.*, 2006, **128**, 6870.
24 X. Qian and Y. Xiao, *Tetrahedron Lett.*, 2002, **43**, 2991.
25 J. F. Hartwig, *Angew. Chem. Int. Ed.*, 1998, **37**, 2046.
26 Z. Wang, C. Kim, A. Facchetti and T. J. Marks, *J. Am. Chem. Soc.*, 2007, **129**, 13362.

27 S. Amin, G. Balanikas, K. Huie, N. Hussain, J. E. Geddie and S. S. Hecht, *J. Org. Chem.*, 1985, **50**, 4642.
28 K.-R. Wee, H.-C. Ahn, H.-J. Son, W.-S. Han, J.-E. Kim, D. W. Cho and S. O. Kang, *J. Org. Chem.*, 2009, **74**, 8472.
29 B. Yang, S.-K. Kim, H. Xu, Y. Park, H. Zhang, C. Gu, F. Shen, C. Wang, D. Liu, X. Liu, M. Hanif, S. Tang, W. Li, F. Li, J. Shen, J.-W. Park and Y. Ma, *ChemPhysChem*, 2008, **9**, 2601.
30 K. R. J. Thomas, T.-H. Huang, J. T. Lin, S.-C. Pu, Y. M. Cheng, C. C. Hsieh and C. P. Tai, *Chem. Eur. J.*, 2008, **14**, 11231.
31 K. R. J. Thomas, A. L. Thompson, A. V. Sivakumar, C. J. Bardeen and S. Thayumanavan, *J. Am. Chem. Soc.*, 2005, **127**, 373.
32 Q.-X. Tong, S.-L. Lai, M.-Y. Chan, Y.-C. Zhou, H.-L. Kwong, C.-S. Lee, S.-T. Lee, T.-W. Lee, T. Noh and O. Kwon, *J. Phys. Chem. C*, 2009, **113**, 6227.
33 K. R. J. Thomas, J. T. Lin, Y.-T. Tao and C.-H. Chuen, *Chem. Mater.*, 2002, **14**, 3852.
34 E. Balasubramaniam, Y.-T. Tao, A. Danel and P. Tomasik, *Chem. Mater.*, 2000, **12**, 2788.
35 M. J. Frisch, G. W. Trucks, H. B. Schlegel, G. E. Scuseria, M. A. Robb, J. R. Cheeseman, G. Scalmani, V. Barone, B. Mennucci, G. A. Petersson, H. Nakatsuji, M. Caricato, X. Li, H. P. Hratchian, A. F. Izmaylov, J. Bloino, G. Zheng, J. L. Sonnenberg, M. Hada, M. Ehara, K. Toyota, R. Fukuda, J. Hasegawa, M. Ishida, T. Nakajima, Y. Honda, O. Kitao, H. Nakai, T. Vreven, J. A. Montgomery, Jr., J. E. Peralta, F. Ogliaro, M. Bearpark, J. J. Heyd, E. Brothers, K. N. Kudin, V. N. Staroverov, R. Kobayashi, J. Normand, K. Raghavachari, A. Rendell, J. C. Burant, S. S. Iyengar, J. Tomasi, M. Cossi, N. Rega, J. M. Millam, M. Klene, J. E. Knox, J. B. Cross, V. Bakken, C. Adamo, J. Jaramillo, R. Gomperts, R. E. Stratmann, O. Yazyev, A. J. Austin, R. Cammi, C. Pomelli, J. W. Ochterski, R. L. Martin, K. Morokuma, V. G. Zakrzewski, G. A. Voth, P. Salvador, J. J. Dannenberg, S. Dapprich, A. D. Daniels, O. Farkas, J. B. Foresman, J. V. Ortiz, J. Cioslowski and D. J. Fox, *GAUSSIAN 09 (Revision A.1)*, Gaussian, Inc., Wallingford, CT, 2009.
36 R. C. Chiechi, R. J. Tseng, F. Marchioni, Y. Yang and F. Wudl, *Adv. Mater.*, 2006, **18**, 325.

